LETTERS

Dendritic encoding of sensory stimuli controlled by deep cortical interneurons

Masanori Murayama[1], Enrique Pérez-Garci[1], Thomas Nevian[1], Tobias Bock[1], Walter Senn[1] & Matthew E. Larkum[1]

The computational power of single neurons is greatly enhanced by active dendritic conductances[1] that have a large influence on their spike activity[2–4]. In cortical output neurons such as the large pyramidal cells of layer 5 (L5), activation of apical dendritic calcium channels leads to plateau potentials that increase the gain of the input/output function[5] and switch the cell to burst-firing mode[6–9]. The apical dendrites are innervated by local excitatory and inhibitory inputs as well as thalamic[10–13] and corticocortical projections[14–16], which makes it a formidable task to predict how these inputs influence active dendritic properties *in vivo*. Here we investigate activity in populations of L5 pyramidal dendrites of the somatosensory cortex in awake and anaesthetized rats following sensory stimulation using a new fibre-optic method[17] for recording dendritic calcium changes. We show that the strength of sensory stimulation is encoded in the combined dendritic calcium response of a local population of L5 pyramidal cells in a graded manner. The slope of the stimulus–response function was under the control of a particular subset of inhibitory neurons activated by synaptic inputs predominantly in L5. Recordings from single apical tuft dendrites *in vitro* showed that activity in L5 pyramidal neurons disynaptically coupled via interneurons directly blocks the initiation of dendritic calcium spikes in neighbouring pyramidal neurons. The results constitute a functional description of a cortical microcircuit in awake animals that relies on the active properties of L5 pyramidal dendrites and their very high sensitivity to inhibition. The microcircuit is organized so that local populations of apical dendrites can adaptively encode bottom-up sensory stimuli linearly across their full dynamic range.

To explore how dendritic activity encodes sensory input *in vivo*, we used a microendoscopic technique (the 'periscope' method[17]) ideal for recording from local populations of L5 pyramidal dendrites in anaesthetized and awake animals (Fig. 1a, Methods). This method provides calcium fluorescence signals exclusively from pyramidal apical tuft dendrites by combining two approaches: specific loading of L5 pyramidal dendrites and horizontal imaging of the upper three layers of cortex (Fig. 1a). Fluorescence responses to sensory stimuli were recorded from populations of L5 bolus-loaded dendrites that were not detectable using two-photon imaging from individual dendrites[18] ($n = 6$, data not shown; see also Methods). This method has a high sensitivity to dendritic activity and can be easily applied to awake, freely moving animals.

Air-puff stimulation of the hindlimb under urethane anaesthesia produced biphasic responses in dendrites of the contralateral hindlimb area of the primary somatosensory cortex (Fig. 1b, black). This dendritic population response could be blocked completely by the application of the Ca^{2+} channel blocker Cd^{2+} to the cortical surface (Fig. 1b, grey), leaving no detectable movement artefacts. Application of the $GABA_A$ (GABA, γ-aminobutyric acid) receptor antagonist, gabazine, to the cortical surface increased the first component of the dendritic population response approximately fivefold ($0.42 \pm 16\%$ versus $2.12 \pm 0.60\%$ (all data given as mean ± s.d.), $P < 0.05$, $n = 5$; Fig. 1b, c, red), whereas the $GABA_B$ receptor antagonist CGP52432 did not change this component ($0.42 \pm 0.16\%$ versus $0.38 \pm 0.07\%$, $P = 0.29$, $n = 5$; Fig. 1b, c, green). Throughout this study we focused on the factors influencing the increase in the initial component of calcium influx into the dendrites modulated by $GABA_A$ receptors.

We investigated the dendritic encoding of stimulus strength using single electrical stimuli to the hindlimb, for which the strength could be reliably and precisely determined. Increasing stimulus strength under urethane anaesthesia resulted in a progressive increase in the population dendritic calcium response ($n = 21$; Fig. 1d; see Supplementary Fig. 1 for $\Delta F/F$ peak amplitude). Blockade of GABA receptors dramatically increased the dendritic population response ($n = 6$; Fig. 1d, e, red), possibly also because of runaway cortical excitation. Blockade of $GABA_B$ receptors alone had very little effect ($n = 6$; Fig. 1e, green). Normalization to the maximal dendritic response in each condition revealed that the responses to increasing stimulus strength were nearly linear under control conditions but highly nonlinear ('all or none') without $GABA_A$ receptor activity (Fig. 1f).

Conscious perception involves a combination of feed-forward and feedback processes[19] that may specifically influence dendritic encoding. To examine dendritic sensory-evoked responses in awake animals, we used a custom-built head mount to stabilize the fibre-optic cable[17]. As in the anaesthetized state, we found that increasing stimulus strength resulted in a graded increase in the population dendritic calcium response ($n = 3$; Fig. 1g). This shows that the mechanisms controlling the linear encoding of dendritic responses to sensory stimulus strength are not affected by anaesthesia. Thus, we continued our experiments to understand in detail what neural mechanisms underlie the change in linearity and dynamic range in anaesthetized animals.

We next investigated the source of dendritic Ca^{2+}. Application of D(-)-2-amino-5-phosphonovaleric acid (APV, to block NMDA receptors) to the cortical surface did not alter the amplitude of the dendritic population signal, indicating negligible contribution by subthreshold Ca^{2+} entry (that is, excitatory postsynaptic potentials (EPSPs)) as shown previously[17] ($P > 0.1$, $n = 6$; Supplementary Fig. 2). However, actively propagated action potentials from the soma into the apical dendrite can cause moderate increases in intracellular calcium concentration ($[Ca^{2+}]_i$), and dendritic Ca^{2+} spikes cause a large signal that is easily detectable[17]. There was no way to directly estimate action potential firing with the periscope method, so we tested the contribution of back-propagating action potentials (BPAPs) to the sensory-evoked dendritic calcium signals by injecting TTX (a Na^+ channel blocker) into L5 (Fig. 2a). Surprisingly, blocking activity in L5 and preventing BPAPs did not decrease the dendritic signal but rather increased it threefold ($1.2 \pm 0.61\%$ versus

[1]Physiologisches Institut, Universität Bern, Bühlplatz 5, CH-3012 Bern, Switzerland.

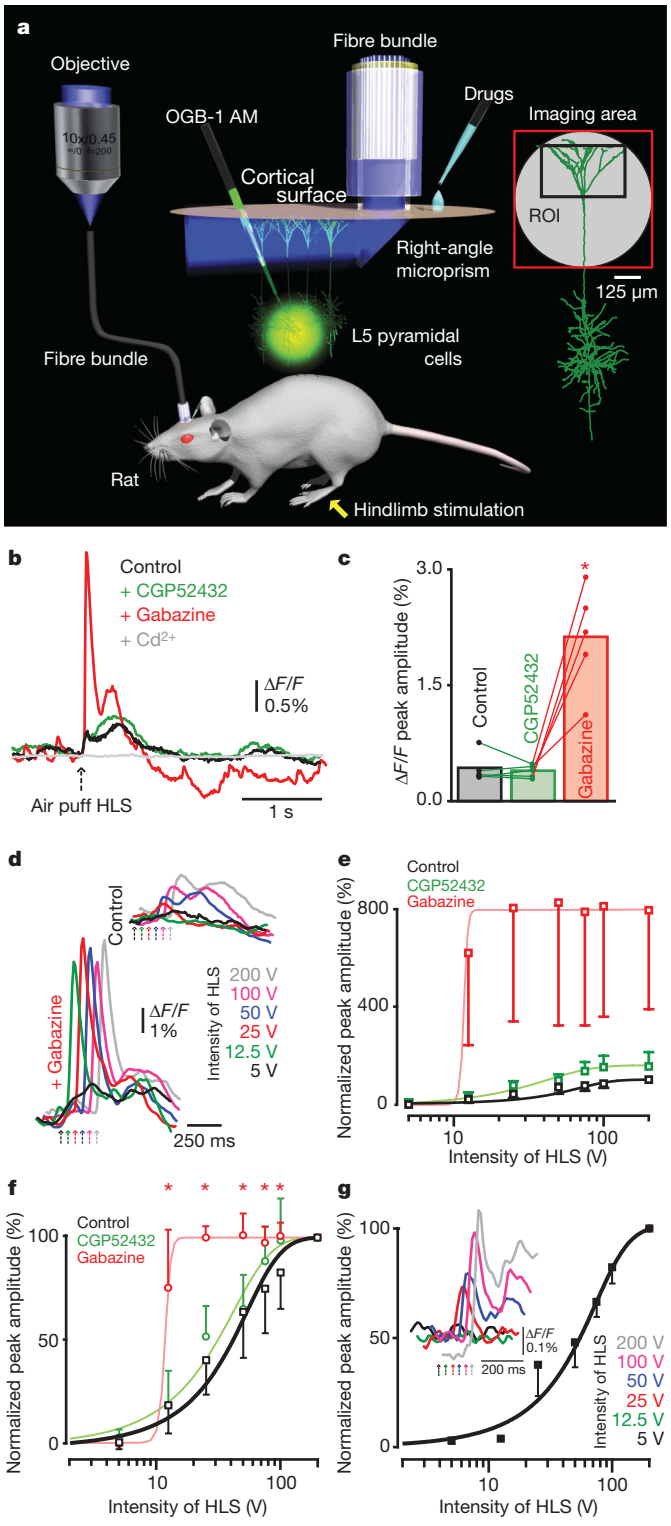

Figure 1 | Graded dendritic population Ca^{2+} responses to somatosensory inputs in anaesthetized and awake rats. **a**, Sketch of the experimental design using the periscope for recording specifically from the apical tuft dendrites of L5 neocortical pyramidal neurons[17]. Right: reconstructed pyramidal cell from *in vitro* experiments, demonstrating the typical regions of the dendritic tree within the imaging area. **b**, Averaged dendritic Ca^{2+} population signals (relative fluorescence change, $\Delta F/F$; 15 trials) recorded with the periscope following contralateral hindlimb stimulation with an air puff in anaesthetized rats (1 µM CGP52432, 3 µM gabazine and 1 mM Cd^{2+} applied to cortical surface). **c**, Summary of **b** ($n = 5$). Circles show the experiments and bars indicate their averages. **d**, Top: Averaged traces (15 trials) showing increase of dendritic Ca^{2+} signals following increase in contralateral electrical stimulation (arrows indicate the stimulus timing, time-shifted for clarity) of the hindlimb with increasing intensities (5–200 V) under control conditions. Bottom: same, after blockade of all GABA receptors. **e**, Summary of **d** ($n = 21$ for control, $n = 6$ for CGP52432 and gabazine; unpaired *t*-tests) fitted with sigmoidal curves with normalized data to maximal control value (200 V). **f**, Summary of **d** with data normalized to maximum in each condition (200 V). **g**, Summary of awake experiments ($n = 3$). Inset, averaged traces of dendritic Ca^{2+} signals in an awake animal. HLS, hindlimb stimulation; ROI, region of interest. $^*P < 0.05$. Error bars, s.d.

3.3 ± 0.95%, $P < 0.05$, $n = 5$; Fig. 2b, e) and changed the biphasic nature of the dendritic response. This result shows first that the large calcium responses detected are dependent on neither dendritic BPAPs nor axonal action potentials and second that an additional TTX-sensitive mechanism in L5 suppresses dendritic $[Ca^{2+}]_i$.

The most likely explanation is that TTX also blocked some inhibitory neurons in L5. Recent studies *in vitro* have shown that inhibition of pyramidal dendrites can be evoked by activation of dendrite-targeting Martinotti interneurons by neighbouring pyramidal neurons[20,21]. To test this possibility, we suppressed the activation of this form of disynaptic inhibition by local injection of CNQX (an antagonist of α-amino-3-hydroxy-5-methyl-4-isoxazole propionic acid (AMPA) receptors and kainate receptors) to L5 (see also Fig. 3). Again, the combined dendritic signal increased (0.61 ± 0.19% versus 0.99 ± 0.36%, $P < 0.05$, $n = 5$; Fig. 2c, f). Even more importantly, blockade of both L5 activity using TTX and disynaptic connectivity using CNQX had exactly the same effect on the slope of the dendritic response curve as a function of stimulus strength (Fig. 2h; see Supplementary Fig. 3 for $\Delta F/F$ peak amplitude). We conclude that deep cortical interneurons control dendritic encoding of sensory inputs.

This conclusion was further supported by the counterintuitive action of gabazine when applied locally to L5, which decreased the dendritic Ca^{2+} signal by nearly 40% (0.76 ± 0.46% versus 0.45 ± 0.30%, $P < 0.05$, $n = 5$; Fig. 2d, g, h). This is consistent with the hypothesis that disinhibition of L5 cells leads to an increase in dendritic inhibition in the upper layers. Moreover, muscimol (a $GABA_A$ receptor agonist) application to L5 increased the signals evoked by hindlimb stimulations (0.59 ± 0.36% versus 0.78 ± 0.46%, $P < 0.05$, $n = 4$; Fig. 2i), whereas muscimol application to layer 1 (L1) decreased dendritic Ca^{2+} signals (0.89 ± 0.47% versus 0.63 ± 0.39%, $P < 0.05$, $n = 4$; Fig. 2i). This experiment suggests that inhibition is mainly dendritic, not perisomatic, which was confirmed with muscimol *in vitro* ($n = 3$, Supplementary Fig. 4). Last, these experiments demonstrate that this form of cortical inhibition predominates over increased firing in pyramidal neurons and increases in recurrent activity.

We next investigated the mechanisms underlying inhibitory control of dendritic activity. For this, we examined whether disynaptically evoked inhibition is sufficient to block dendritic Ca^{2+} spikes. We performed triple-patch recordings *in vitro* from pairs of disynaptically coupled L5 pyramidal neurons[20] (Fig. 3a) with the third recording in the dendritic Ca^{2+} spike initiation zone 500–800 µm from the cell body ($n = 3$, Fig. 3a). Trains of 18–20 action potentials at 80–100 Hz in the presynaptic pyramidal neuron evoked disynaptic dendritic inhibition (Fig. 3b). Dendritic Ca^{2+} spikes evoked with dendritic current injection (Fig. 3c) could be completely abolished by the disynaptically evoked dendritic inhibition in an all-or-none fashion (Fig. 3d). The same phenomenon could be observed with calcium imaging of the Ca^{2+} spike initiation zone. Disynaptically evoked inhibition severely reduced the Ca^{2+} fluorescence due to Ca^{2+} spikes into this region evoked with high-frequency trains of back-propagating action potentials[22] (23.0 ± 19.8%, $P < 0.05$, $n = 3$; Fig. 3e–g; for details, see Supplementary Fig. 5). The effect of disynaptic inhibition was blocked by local application of CNQX to L5 analogous to the *in vivo* experiments ($n = 3$). The strongest blockade of inhibition occurred when CNQX was puffed close to L5 ($n = 3$, Fig. 3h–j), implying that most of the disynaptic dendritic inhibition is evoked by cells in lower cortical layers.

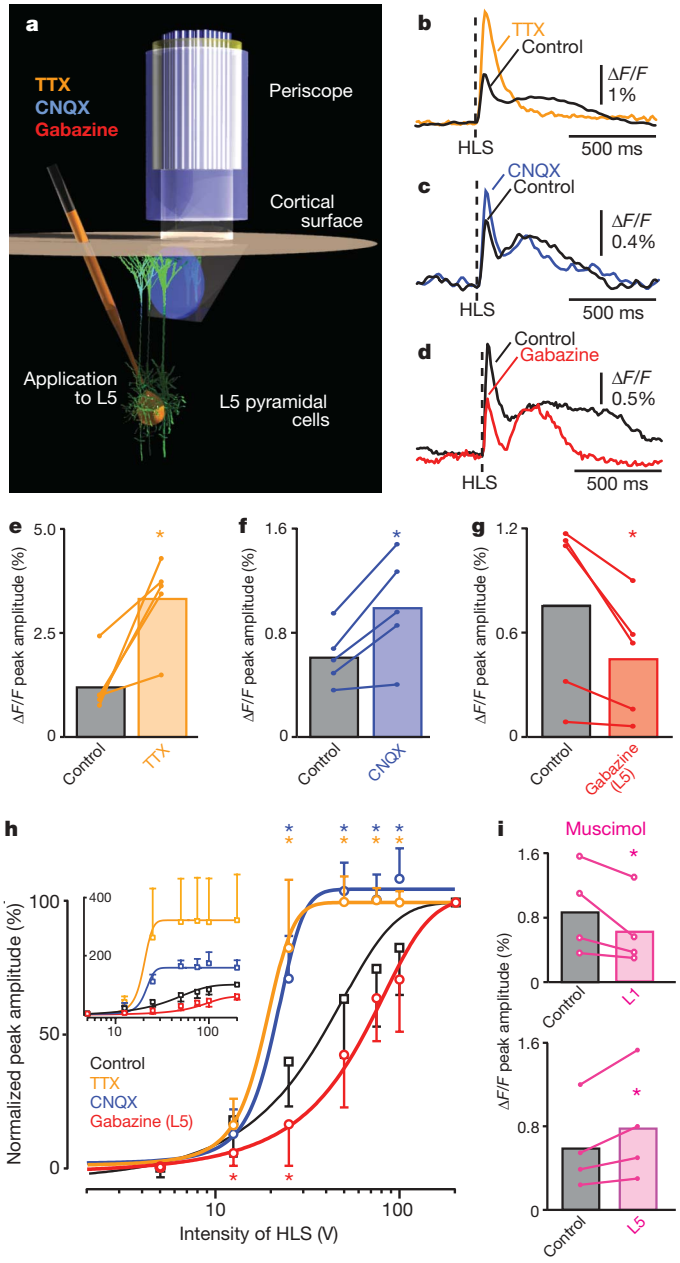

Figure 2 | Deep-layer control of dendritic activity. **a**, Sketch showing local application of tetrodotoxin (TTX, 3 μM), 6-cyano-7-nitroquinoxaline-2,3-dione (CNQX, 100 μM) and gabazine (1 μM) injected into L5. **b**–**d** Averaged responses (15 trials) in single animals. **e**–**g**, Summary of **b**–**d** ($n = 5$ for each drug). **h**, Responses (normalized to maximum of each condition) versus stimulus strength in control ($n = 21$), with TTX ($n = 5$), CNQX ($n = 5$) and gabazine ($n = 5$). Asterisks indicate significance with unpaired t-tests. Inset, data normalized to control. **i**, Summary of muscimol injection to L1 (top, $n = 4$) and to L5 (bottom, $n = 4$). Application of normal rat ringer to L5 and L1 did not change evoked Ca^{2+} signals (0.83 ± 0.76% for control versus 0.76 ± 0.49% for L5 and 0.77 ± 0.46% for L1, $n = 3$). *$P < 0.05$. Error bars, s.d.

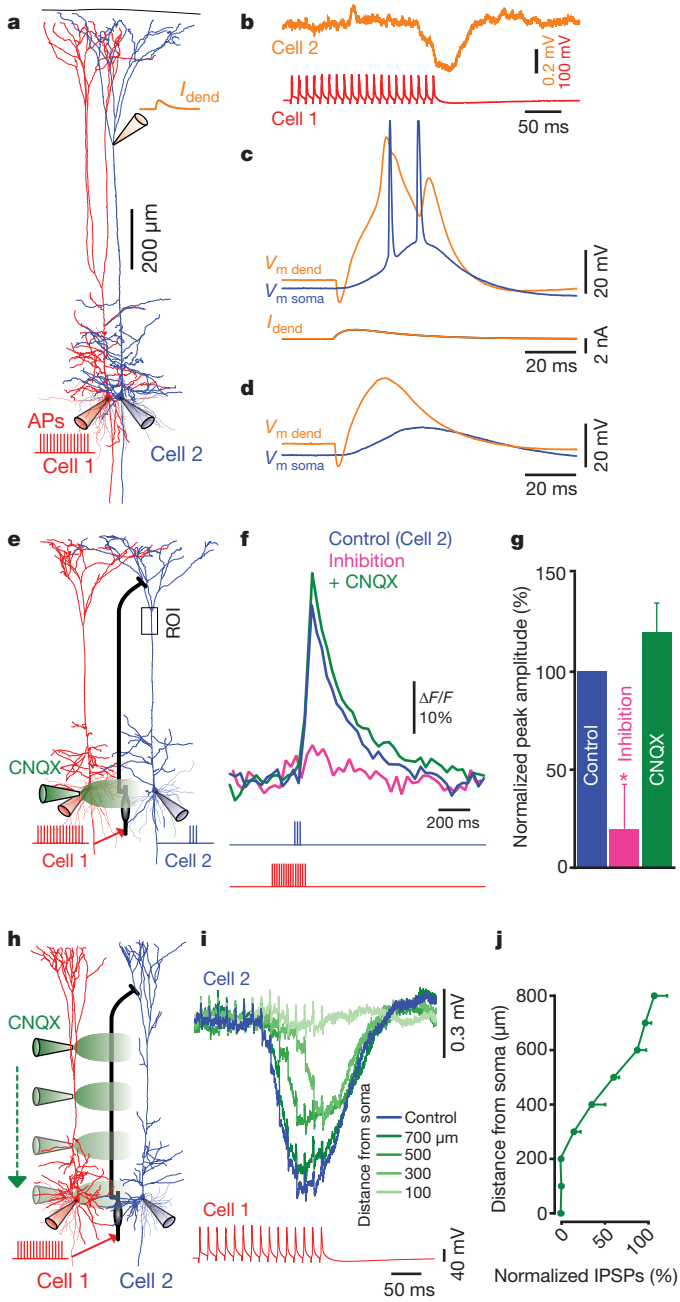

Figure 3 | Disynaptic inhibition blocks dendritic Ca^{2+} spikes *in vitro*. **a**, Experimental diagram showing reconstructed L5 somatosensory pyramidal neurons and recording sites. **b**, Averaged disynaptically evoked inhibitory postsynaptic potential (IPSP) (15 sweeps). **c**, Dendritic Ca^{2+} spike ($V_{m\ dend}$) evoked by dendritic current injection (I_{dend}) caused a burst of somatic action potentials ($V_{m\ soma}$). **d**, Same as **c**, but with disynaptic inhibition. **e**, Experimental diagram. Pyramidal neurons were artificially separated and the putative interneuron (black) added schematically. Cell 2 was filled with OGB-1 (100 μM) and Ca^{2+} fluorescence ($\Delta F/F$) measured at a distal ROI. CNQX (20 μM) was applied 100 μm from the soma. **f**, Ca^{2+} fluorescence transients (blue) were blocked by disynaptic inhibition (pink) and recovered with local application of CNQX (green). **g**, Summary of **f** ($n = 3$). **h**, Experimental diagram. CNQX was applied at nine locations 100 μm apart in the vertical axis. **i**, Averaged IPSP (30 sweeps) recorded in cell 2 evoked by a train of presynaptic action potentials in cell 1. **j**, Summary of **i** ($n = 3$). AP, action potential. *$P < 0.05$. Error bars, s.d.

The experiments show that very specific cortical microcircuitry is involved in determining the responsiveness of apical dendrites of L5 pyramidal neurons (Fig. 4a). Both the *in vivo* and the *in vitro* data suggest that individual dendritic Ca^{2+} signals contribute to the population responses by means of all-or-none Ca^{2+} spikes consistent with previous recordings *in vivo*[8,23], and that the inhibition of dendritic Ca^{2+} spikes is also all or none[24,25]. To investigate how the microcircuitry shapes the grading of the dendritic population response, we modelled a population of two-compartment pyramidal neurons[5] receiving distributed feed-forward and feedback excitation and inhibition (Fig. 4b; see Methods and Supplementary Information, model description). The distribution of Ca^{2+} spike thresholds in the dendritic compartments (Fig. 4c, d, green) was chosen to allow for a steep all-or-none Ca^{2+} population response when dendritic

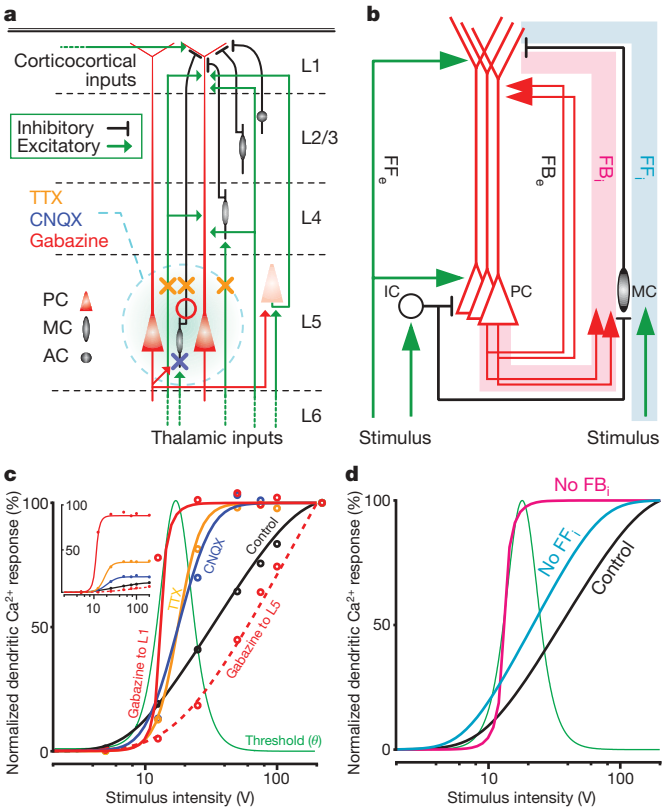

Figure 4 | Model of microcircuitry with all-or-none dendritic Ca^{2+} spikes. **a**, Diagram of cortical circuitry. The blue shaded region indicates the elements in the circuit affected by TTX, CNQX and gabazine. PC, pyramidal cell; MC, Martinotti cell; AC, aspiny cell. **b**, Model microcircuitry with a population of two-compartment pyramidal neurons with all-or-none dendritic Ca^{2+} events and four major classes of dendritic inputs (FF_e, feed-forward excitation; FF_i, feed-forward inhibition; FB_e, feedback excitation; FB_i, feedback inhibition; Blue and green arrows, excitation; black lines, inhibition). Dendritic feed-forward inhibition and feedback inhibition both act through deep-layer Martinotti cells (red and blue stripes). IC, inhibitory cell. **c**, Data fitted with the model by mimicking the pharmacological blocking experiments in L5 and L1 (see Supplementary Information, model description). Inset, model responses scaled to the number of neurons in the population recruitable for Ca^{2+} spikes. **d**, Effects of blocking feedback and feed-forward inhibition, respectively (see text and also Supplementary Fig. 10, which shows the effect of changing the strength of inhibition on the slope).

inhibition is blocked (for example for gabazine to the cortical surface; Fig. 4c). The dendritic population response curves for the pharmacological blocking experiments could be reproduced by removing the corresponding model connectivity to upper and lower layers, respectively (Fig. 4b, c). The model also predicts that blocking the feed-forward drive onto the inhibitory Martinotti cells[26] merely shifts the response curve to the left by reducing its threshold (Fig. 4d, light blue), whereas blocking feedback inhibition[20,21] increases the gain of the response curve and thus modulates the dynamic range of the population calcium response (Fig. 4d, pink; see Supplementary Fig. 11 for further details).

We conclude that the representation of sensory stimuli by cortical output neurons cannot be fully explained by the traditional axosomatic integration approach, but requires active dendrites embedded within highly specialized cortical microcircuitry. Dendritic activity is tightly controlled by interneurons projecting from deep to upper layers (Martinotti cells) whose function was previously unknown. We show here that these neurons dynamically modulate the slope and threshold of the dendritic response function to match the physiologically relevant input range.

METHODS SUMMARY

Female Wistar rats (24–40 d old) were used for these experiments. Multiple dendrites of L5 pyramidal cells were loaded with a Ca^{2+}-sensitive dye, Oregon Green 488 BAPTA-1 AM (OGB-1 AM), by means of bolus injection to L5 (ref. 17). Fibre-optic calcium imaging *in vivo* was performed in the primary somatosensory cortex of awake and urethane-anaesthetized rats as described previously[17] (Fig. 1). Briefly, we used a custom-built microscope attached to a fibre-optic cable (IGN-06/17, 680-μm diameter, Sumitomo Electric Industries). A GRIN lens, right-angled prism (500 × 500 μm; GrinTech) assembly was attached to the end of the fibre and the prism inserted into the hindlimb area of the somatosensory cortex (determined beforehand with intrinsic imaging). Sensory responses were evoked by brief air puffs (50-ms duration) delivered to the contralateral hindlimb or a single short electrical microstimulation pulse (0.1-ms duration, 5–200 V) through a surface electrode. All stimuli were below the threshold for muscle responses in the hindlimb. *In vitro* patch-clamp recordings from L5 pyramidal cells were made in parasagittal slices prepared with standard techniques[25]. Statistical analysis was performed with paired *t*-tests unless otherwise noted; asterisks denote $P < 0.05$.

Full Methods and any associated references are available in the online version of the paper at www.nature.com/nature.

Received 31 July; accepted 18 November 2008.
Published online 18 January 2009.

1. London, M. & Häusser, M. Dendritic computation. *Annu. Rev. Neurosci.* **28,** 503–532 (2005).
2. Llinás, R. R. The intrinsic electrophysiological properties of mammalian neurons: insights into central nervous system function. *Science* **242,** 1654–1664 (1988).
3. Johnston, D., Magee, J. C., Colbert, C. M. & Christie, B. R. Active properties of neuronal dendrites. *Annu. Rev. Neurosci.* **19,** 165–186 (1996).
4. Destexhe, A., Mainen, Z. F. & Sejnowski, T. J. Synthesis of models for excitable membranes, synaptic transmission and neuromodulation using a common kinetic formalism. *J. Comput. Neurosci.* **1,** 195–230 (1994).
5. Larkum, M. E., Senn, W. & Lüscher, H.-R. Top-down dendritic input increases the gain of layer 5 pyramidal neurons. *Cereb. Cortex* **14,** 1059–1070 (2004).
6. Schiller, J., Schiller, Y., Stuart, G. & Sakmann, B. Calcium action potentials restricted to distal apical dendrites of rat neocortical pyramidal neurons. *J. Physiol. (Lond.)* **505,** 605–616 (1997).
7. Kim, H. G. & Connors, B. W. Apical dendrites of the neocortex: correlation between sodium- and calcium-dependent spiking and pyramidal cell morphology. *J. Neurosci.* **13,** 5301–5311 (1993).
8. Larkum, M. E. & Zhu, J. J. Signaling of layer 1 and whisker-evoked Ca2+ and Na+ action potentials in distal and terminal dendrites of rat neocortical pyramidal neurons *in vitro* and *in vivo*. *J. Neurosci.* **22,** 6991–7005 (2002).
9. Williams, S. R. & Stuart, G. J. Mechanisms and consequences of action potential burst firing in rat neocortical pyramidal neurons. *J. Physiol. (Lond.)* **521,** 467–482 (1999).
10. White, E. L. & Hersch, S. M. A quantitative study of thalamocortical and other synapses involving the apical dendrites of corticothalamic projection cells in mouse SmI cortex. *J. Neurocytol.* **11,** 137–157 (1982).
11. Hersch, S. M. & White, E. L. Thalamocortical synapses with corticothalamic projection neurons in mouse SmI cortex: electron microscopic demonstration of a monosynaptic feedback loop. *Neurosci. Lett.* **24,** 207–210 (1981).
12. Zhu, Y. & Zhu, J. J. Rapid arrival and integration of ascending sensory information in layer 1 nonpyramidal neurons and tuft dendrites of layer 5 pyramidal neurons of the neocortex. *J. Neurosci.* **24,** 1272–1279 (2004).
13. Oda, S. *et al.* Thalamocortical projection from the ventral posteromedial nucleus sends its collaterals to layer I of the primary somatosensory cortex in rat. *Neurosci. Lett.* **367,** 394–398 (2004).
14. Budd, J. M. L. Extrastriate feedback to primary visual cortex in primates: a quantitative analysis of connectivity. *Proc. R. Soc. Lond. B* **265,** 1037–1044 (1998).
15. Cauller, L. J. & Connors, B. W. Synaptic physiology of horizontal afferents to layer-I in slices of rat SI neocortex. *J. Neurosci.* **14,** 751–762 (1994).
16. Elhanany, E. & White, E. L. Intrinsic circuitry: synapses involving the local axon collaterals of corticocortical projection neurons in the mouse primary somatosensory cortex. *J. Comp. Neurol.* **291,** 43–54 (1990).
17. Murayama, M., Pérez-Garci, E., Lüscher, H. R. & Larkum, M. E. Fiberoptic system for recording dendritic calcium signals in layer 5 neocortical pyramidal cells in freely moving rats. *J. Neurophysiol.* **98,** 1791–1805 (2007).
18. Kerr, J. N., Greenberg, D. & Helmchen, F. Imaging input and output of neocortical networks *in vivo*. *Proc. Natl Acad. Sci. USA* **102,** 14063–14068 (2005).
19. Cauller, L. Layer I of primary sensory neocortex: Where top-down converges upon bottom-up. *Behav. Brain Res.* **71,** 163–170 (1995).
20. Silberberg, G. & Markram, H. Disynaptic inhibition between neocortical pyramidal cells mediated by Martinotti cells. *Neuron* **53,** 735–746 (2007).
21. Kapfer, C., Glickfeld, L. L., Atallah, B. V. & Scanziani, M. Supralinear increase of recurrent inhibition during sparse activity in the somatosensory cortex. *Nature Neurosci.* **10,** 743–753 (2007).

22. Larkum, M. E., Kaiser, K. M. & Sakmann, B. Calcium electrogenesis in distal apical dendrites of layer 5 pyramidal cells at a critical frequency of back-propagating action potentials. *Proc. Natl Acad. Sci. USA* **96,** 14600–14604 (1999).
23. Helmchen, F., Svoboda, K., Denk, W. & Tank, D. W. *In vivo* dendritic calcium dynamics in deep-layer cortical pyramidal neurons. *Nature Neurosci.* **2,** 989–996 (1999).
24. Larkum, M. E., Zhu, J. J. & Sakmann, B. A new cellular mechanism for coupling inputs arriving at different cortical layers. *Nature* **398,** 338–341 (1999).
25. Pérez-Garci, E., Gassmann, M., Bettler, B. & Larkum, M. E. The GABAB1b isoform mediates long-lasting inhibition of dendritic Ca2+ spikes in layer 5 somatosensory pyramidal neurons. *Neuron* **50,** 603–616 (2006).
26. Tan, Z., Hu, H., Huang, Z. J. & Agmon, A. Robust but delayed thalamocortical activation of dendritic-targeting inhibitory interneurons. *Proc. Natl Acad. Sci. USA* **105,** 2187–2192 (2008).

Supplementary Information is linked to the online version of the paper at www.nature.com/nature.

Acknowledgements We thank K. Martin, H.-R. Lüscher and Y. Kudo for their comments on the manuscript, O. Gschwend for support in the laboratory, D. Morris for software development, D. Limoges and J. Burkhalter for their expert technical support and K. Fischer for Neurolucida reconstructions of the biocytin-filled neurons. We also thank Sumitomo Electric Industries for their generous donation of the optical fibre. This work was supported by the Swiss National Science Foundation (grant no. PP00A-102721/1).

Author Contributions M.M. and M.E.L. designed the study. M.M. performed the periscope experiments *in vivo*, E.P.-G. performed the *in vitro* experiments, and T.N. and M.M. performed the *in vivo* two-photon experiments. W.S. and T.B. made the model and the supplementary model description. M.M. and M.E.L. prepared the manuscript.

Author Information Reprints and permissions information is available at www.nature.com/reprints. Correspondence and requests for materials should be addressed to M.E.L. (larkum@pyl.unibe.ch).

METHODS

The following methods have already been mostly described in ref. 17.

Animals and surgery. Female Wistar rats (P24–P40) were used in these experiments. Urethane (intraperitoneal, 1.5 g kg^{-1}) was used for experiments under anaesthesia. The head was fixed in a stereotaxic instrument (Model SR-5R, Narishige) and body temperature maintained at 36 to 37 °C. A craniotomy above the primary somatosensory cortex (3 × 4.4 mm square), centred at 1.5 mm posterior to bregma and 2.2 mm from midline in the right hemisphere, was performed and the dura mater surgically removed immediately before Ca^{2+} recording (see below). For awake experiments, the scalp was removed under general anaesthesia (isoflurane, Baxter) and a local anaesthetic (lidocaine; Sigma-Aldrich) was applied to the wound. Following surgery, an analgesic was administered (buprenorphine (twice per day), Essex Chemie) and local anaesthetic applied to the scalp. On the day of the experiment, a craniotomy was performed, a Ca^{2+}-sensitive dye was injected into L5 (see below) and a metal post was fixed to the skull with dental cement. After anaesthesia, the animals were retrained in a holder (Clam005, Kent Scientific).

***In vivo* loading of Ca^{2+}-sensitive dye.** Oregon Green 488 BAPTA-1 (OGB-1) AM (50 μg; Molecular Probes) was mixed with 5 μl of pluronic acid (Pluronic F-127, 20% solution in dimethylsulphoxide; Molecular Probes) for 15 min. The solution was then diluted in 28 μl of HEPES-buffered solution (125 mM NaCl, 2.5 mM KCl, 10 mM HEPES) and mixed for a further 15 min. The OGB-1 AM solution was loaded into a glass pipette (tip diameter, 5–20 μm) and pressure-injected into L5 (pressure, 10–25 kPa) for 1 min. The pipette was withdrawn and the area of the craniotomy was then submerged with rat ringer (135 mM NaCl, 5.4 mM KCl, 1.8 mM CaCl2, 1 mM MgCl2, 5 mM HEPES) for 2 h.

***In vivo* Ca^{2+} recording (periscope).** A 100-W mercury lamp (U-LH100HG, Olympus) or a blue light-emitting-diode (LED, IBF+LS30W-3W-Slim-RX, Imac) was used as a light source. An excitation filter, a dichroic mirror, and an emission filter (as a filter set 31001, Chroma Technology) were used for epifluorescence Ca^{2+} recordings. A ×10 objective (0.45 numerical aperture, Model E58-372, Edmund Optics) was used for illuminating and imaging a fibre bundle (see below). A cooled charge-coupled-device (CCD) camera (MicroMax, Roper Scientific) was used for collecting fluorescence.

A fibre bundle (IGN-06/17, Sumitomo Electric Industries) consisting of 17,000 fibre elements was used as a combined illuminating–recording fibre. The end face of the bundle was fitted with a prism-lens assembly that consisted of a right-angled prism (0.5 × 0.5 × 0.5 mm; GrinTech) attached to a GRIN lens (diameter, 0.5 mm; 0.5 numerical aperture; GrinTech). The working distance was nominally 100 μm and the magnification was ×0.73, resulting in a field of view of 685-μm diameter.

Sensory responses were evoked by a brief air puff (50-ms duration) delivered to the contralateral hindlimb or a single short electrical stimulation (0.1-ms duration, 5–200 V). Fluorescence changes were sampled at 100 Hz. Data were acquired on a personal computer using WinView software (Roper Scientific). Regions of interest were chosen offline for measuring fluorescence changes (see data analysis section). Gabazine and CGP52432 were bought from Biotrend Chemicals, tetrodotoxin (TTX) from Tocris Cookson and cadmium chloride from Fluka.

***In vivo* Ca^{2+} recording (two-photon).** Two-photon excitation fluorescence microscopy was either performed with a femtosecond infrared laser (λ = 800–810 nm, 100 fs; Tsunami pumped by a Millennia VIII or Mai-Tai HP, Spectra-Physics) coupled to a laser scanning microscope (TCS SP2RS, Leica) equipped with a ×40 water immersion objective (HCX APO w40x, UVI, numerical aperture 0.8) or a custom-built two-photon microscope equipped with a ×20 water immersion objective (numerical aperture 0.95; Olympus). Excitation infrared-laser light and fluorescence-emission light were separated at 670 nm (excitation filter 670DCXXR, AHF Analysentechnik) and the infrared light was blocked in the detection pathway with an infrared-block filter (E700SP, AHF Analysentechnik). Fluorescence was detected using epifluorescence non-descanned detection. Calcium transients were recorded in line-scan mode at 500 Hz from identified L5 tuft dendrites.

***In vitro* experiments.** Animals were anaesthetized with a mixture of 95% CO_2/5% O_2 before decapitation. The brain was then rapidly transferred to ice-cold, oxygenated artificial cerebrospinal fluid (ACSF) containing 125 mM NaCl, 25 mM $NaHCO_3$, 2.5 mM KCl, 1.25 mM NaH_2PO_4, 1 mM $MgCl_2$, 25 mM glucose and 2 mM $CaCl_2$ (pH 7.4). Parasagittal slices of the primary somatosensory cortex (300-μm thick) were cut with a vibrating microslicer on a block angled at 15° to the horizontal and maintained at 37 °C in the preceding solution for 15–120 min before use.

Ca^{2+} imaging and somatic whole-cell patch recordings of L5 neurons were obtained with Nikon Eclipse E600FN microscopes (Nikon). Ca^{2+} imaging was performed using a CCD camera (CoolSNAP, Roper Scientific). The fluorescence was observed using standard epifluorescence filter sets for fluorescein (excitation at 480 nm; used for OGB-1) and Texas Red (Alexa 594; Molecular Probes) fluorescence (Chroma Technology). Fluorescence intensities were sampled at 30–40 Hz. Pipettes (4–6 MΩ) for the whole-cell patch-clamp recordings were filled with an intracellular solution containing 135 mM K-gluconate, 7 mM KCl, 10 mM HEPES, 10 mM Na_2-phosphocreatine, 4 mM Mg-ATP, 0.3 mM GTP, 10 mM Alexa 594 and 0.2% biocytin (pH 7.2 with KOH). No correction was made for the junction potential between the bath and pipette solutions. The recordings were made with Multiclamp 700B (Axon Instruments), digitized at 10 kHz with an analogue–digital converter (ITC-16 Instrutech) and acquired on a personal computer using Igor software (WaveMetrics). Dendritic Ca^{2+} spikes were evoked with EPSP-shaped current waveforms injected through a dendritic pipette: double exponential, $f_{(t)} = (1 - e^{-t/\tau_1})e^{-t/\tau_2}$, where $\tau_1 = 4$ ms and $\tau_2 = 10$ ms; time to peak, 5 ms. Slices were perfused continuously with the ACSF at 33–35 °C throughout the experiments.

Data analysis. The fluorescence signals *in vivo* were quantified by measuring the mean pixel value of a manually selected (offline) ROI for each frame of the image stack using Igor software. Ca^{2+} changes were expressed as $\Delta F/F = F_t/F_0$, where F_t was the average fluorescence intensity within the ROI at time t during the imaging experiment and F_0 was the mean value of fluorescence intensity before stimulation. For *in vitro* experiments, Ca^{2+} changes were expressed as $\Delta F/F = (F_t - F_0)/(F_0 - F_B)$, where F_B is the background fluorescence measured from a region away from the recorded area.

Model. The full model comprises microcircuitry with two types of inhibitory neuron and a population of N two-compartment pyramidal neurons displaying all-or-none dendritic calcium events (0 or c). The mathematical analysis of the microcircuitry leads to a compact description of the population calcium response, $C(S)$, as a function of the stimulus strength, S, and the feed-forward and feedback connection strengths $\beta^{ff} = FF_e - FF_i$ and $\beta^{fb} = FB_e - FB_i$, respectively. We fit the distribution of the calcium activation thresholds (mean, θ_0; standard deviation, σ) such that the steep response curve for TTX (modelled by $\beta^{fb} = 0$) is reproduced. The population calcium response can be approximated by the sigmoidal function

$$C(S) \approx \frac{Nc}{1 + \exp(-\gamma(\beta^{ff} \log S - (\theta_0 + \theta_1))/\sigma)}$$

with gain factor $\gamma = (1 - \beta^{fb}c/4\sigma)^{-1}$ and threshold shift $\theta_1 = -\beta^{fb}c/2$; see Supplementary Information, model description. The pharmacological blocking experiments are described by assuming that the corresponding model connections are removed (Fig. 4b, c), and this changes the values of β^{ff} and β^{fb}. Roughly speaking, these experiments lead to an increase in β^{fb} (CNQX, TTX, gabazine to L1) with a corresponding gain increase, and to a reduction in β^{ff} (gabazine to L5) with a corresponding rightwards shift of the $C(S)$ curve. Analogously, blocking the feed-forward excitation of the (inhibitory) model Martinotti cells increases β^{ff} and leads to a leftwards shift of $C(S)$, whereas blocking the Martinotti cell output increases β^{fb} and leads to a gain increase (blue and pink curves in Fig. 4d). The number of pyramidal neurons, N, that can be recruited to contribute to the population calcium signal is a nonlinearly increasing function of the dendritic feedback strength β^{fb} and a linearly increasing function of the gain factor γ (see Supplementary Information, model description).